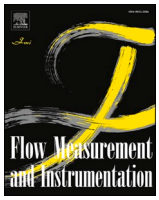
Flow Measurement and Instrumentation 94 (2023) 102476



Contents lists available at ScienceDirect

Flow Measurement and Instrumentation

journal homepage: www.elsevier.com/locate/flowmeasinst



Computational fluid dynamics analysis of flowmeters with elliptical gear pairs and evaluation of calculated flow rate by Taguchi method☆

İbrahim Pazarkaya [a,*], Mehmet Yazar [b], Ahmet Özdemir [c]

[a] Graduate School of Natural and Applied Sciences, Gazi University, Ankara, 06500, Turkiye
[b] Çanakkale Vocational School of Technical Sciences, Çanakkale Onsekiz Mart University, Çanakkale, 17020, Turkiye
[c] Faculty of Technology, Gazi University, Ankara, 06500, Turkiye

ARTICLE INFO

Keywords:
Elliptical gear
Ansys-Fluent
Taguchi
Flowmeter
CFD

ABSTRACT

Accurate determination of flowmeters' design and manufacturing parameters ensures that commercially available flowmeters' declared characteristics are reliable. In this study, nine different flow meters with elliptical gear pairs were manufactured at three different a/b ratios, three different modules, and three different tooth numbers, and the Computational Fluid Dynamics (CFD) models were prepared. CFD analysis forms the basis of the study's methodology, which seeks to statistically identify the most appropriate elliptical gear parameters according to the flow meters manufactured and what the most influential parameter that changes the measured flow rate is. As the pressure of the fluid increased, the measured and CFD-calculated flow rates decreased. According to the measured flow rates and CFD analysis results, it was found that the average flow rate change was −0.0102 %, the biggest change was in the flow meter coded Db-03 with 0.0855 % at 3.00 MPa pressure, and the least change was in the flow meter coded Db-02 with 0.0002 % at 4.50 MPa pressure. The CFD models developed for the manufactured flowmeters were suitable for all flowmeters according to the measured and calculated percent flow rate variations. Taguchi L_9 analysis revealed that a/b = 1.40, m = 2.50 mm, and z = 40 teeth are the optimal manufacturing parameters for elliptical gear, according to the signal-to-noise ratio based on the largest, best analysis. According to the analysis of variance, the modulus value contributed the most to the calculated flow rate at 65.25%, whereas the a/b ratio contributed the least with 0.96%.

1. Introduction

In recent years, the increasing energy demand has necessitated the efficient measurement of the consumption values of liquids and gases. The need to measure the airflow rate to estimate the energy consumption of refrigerated trucks frequently used in tropical regions, get fuel consumption data of tractors in the field of agriculture, and obtain accurate fuel consumption data of ships for engine maintenance programs in the maritime sector has led to the use of elliptical gear flowmeters in such systems, according to many studies that have examined the relevant literature [1–3]. Nevertheless, it was identified that elliptical gear flowmeters can be utilized in place of turbine-type flowmeters for multiphase flow measurements in petroleum fields [4].

An elliptical gear is a type of gear with equally spaced tooth profiles arrayed around a pitch ellipse. This gear type was found to provide a more balanced structure in the acceleration values of the dynamic movements of the rod mechanisms because it satisfies the requirements for high efficiency and precision in mechanical systems, such as clock mechanisms following the orbital motions of Mercury and the Moon, automatic gaming devices, key opening machines, music boxes, pumps, and Geneva mechanisms [5–7]. Elliptical gears are also preferred in textiles, labeling, packaging, and flow meters [8]. In the literature, the geometric and mathematical equations of the pitch ellipse are described in depth, and various equations have been proposed for the accurate calculation of the circumference length of the pitch ellipse in the design and manufacture of elliptical gears [9,10].

The perimeter length of the pitch ellipse can be found by approximate solutions such as Ramanujan's equation [11], and it has been

☆ The authors declare the following financial interests/personal relationships which may be considered as potential competing interests:IBRAHIM PAZARKAYA reports financial support and equipment, drugs, or supplies were provided by Gazi University Scientific Research Projects Coordination Unit. IBRAHIM PAZARKAYA reports writing assistance was provided by Gazi University Academic Writing Application and Research Center.

* Corresponding author.
E-mail address: ipazarkaya@aku.edu.tr (İ. Pazarkaya).

https://doi.org/10.1016/j.flowmeasinst.2023.102476
Received 23 July 2023; Received in revised form 25 September 2023; Accepted 11 October 2023
Available online 12 October 2023
0955-5986/© 2023 Elsevier Ltd. All rights reserved.

established that there are analytical solutions among approximate solutions [12].

Today, it is known that elliptical gear designs can be created in a variety of Computer-Aided Design (CAD) environments. Many theoretical and experimental studies on elliptical gears have also been published, and it has been observed that tooth profiles based on the rolling method with rack-shaped cutting tools can be generated in CAD programs [13–16].

It is also known that elliptical gear pairs are preferred in pumps and flow meters. Some studies have used Particle Image Velocimetry (PIV) to estimate the turbulent kinetic energy dissipation rate, including the spatial derivatives of the velocity fluctuation components of gear pumps [17]. The internal flow characteristics of elliptical gear pumps and flow meters have been the subject of few studies. Computer-Aided Engineering (CAE) programs were utilized to examine the flow characteristics of pumps and flowmeters. The Fluid-Structure Interaction (FSI) analysis of the elliptical gear flowmeter found that the rotor gear's power decreases as the flow rate increases [18].

In another study, the ANSYS Fluent module was used to investigate the working principle of flowmeters with high-order elliptical gears. Under the analysis results, it was determined that a pair of non-circular gears could be added to the system to minimize flow vibration [19].

Similarly, the flow analysis of a pump with an elliptical gear pair in an ANSYS Fluent environment concluded that the output flow rate increases with the rotational speed of the rotor gear and the centrifugal ratio. On the other hand, it is concluded that the effect of the number of teeth on the output flow rate can be neglected [20].

In this research, nine different elliptical gear flowmeters were designed and manufactured using the Taguchi method, and Computational Fluid Dynamics (CFD) models were created. The flow rates obtained from CFD analysis were compared to the experimentally measured flow rates from manufactured flow meters. As a consequence of the comparisons, the parameters of the elliptical gear that provide a correct flow rate were identified. There is no study in the literature on which parameters are the most influential on the flow rates measured by the flowmeters; therefore, the statistical data are presented to figure out these parameters, and a void is attempted to be filled regarding elliptical gear flowmeters.

2. Theoretical analysis of fluid dynamics for elliptical gear flowmeter

Even though the internal flow field and boundary conditions of a flowmeter with an elliptical gear pair are quite complicated, they must satisfy the fundamental fluid control equations, such as the Navier-Stokes and continuity equations. However, solving these equations analytically is challenging. Because of this, modern computer-aided analysis makes it possible to solve equations using various techniques, including finite element, finite difference, finite volume, and spectral methods. This investigation employs the CFD technique of analysis. The Tensor equations [20] used in these analyses are given in Equation (1) and Equation (2).

$$\frac{\partial \rho}{\partial t}+\frac{\partial(\rho u_i)}{\partial x_i}=0 \tag{1}$$

$$\frac{\partial(\rho u_i)}{\partial t}=-\frac{\partial \prod_{ik}}{\partial x_k} \tag{2}$$

for incompressible fluids Π_{ik},

$$\prod_{ik}=-p\delta_{ik}+\eta\left(\frac{\partial u_i}{\partial x_k}+\frac{\partial u_k}{\partial x_i}\right) \tag{3}$$

is obtained. Where p is pressure, and η is dynamic viscosity.

Turbulence occurs during the operation of the elliptical gear flowmeter, particularly in the gear region and internal flow field. The walls of the flowmeter body enclose the fluid, which rotates with the elliptical gears. This indicates that the standard turbulence model fails to represent the flow conditions adequately. Reynolds Averaging of the Navier-Stokes (RANS) equations is one of the most straightforward methods commonly used to simulate turbulent fluid. The standard κ – ε (Launder and Spalding) model was selected because it has been shown to function well in modeling turbulent fluids in gear pumps. According to the physics of turbulent flows, the Realizable κ – ε model satisfies certain mathematical constraints on Reynolds stresses. In deriving the κ – ε model, it is supposed that the flow is solely turbulent and that the effects of molecular viscosity are negligible. The advantage of the Realizable κ – ε model is that it predicts the velocity of both planar and circular streams more correctly. It may also offer superior performance for fluxes involving rotation, boundary layers under strong back pressure gradients, separation, and recirculation [21]. Where κ represents turbulent kinetic energy, and ε represents turbulent dissipation. Equation (4) and Equation (5) illustrate the Realizable κ – ε model [21] equations.

$$\frac{\partial}{\partial t}(\rho\kappa)+\frac{\partial}{\partial x_j}(\rho\kappa u_j)=\frac{\partial}{\partial x_j}\left[\left(\mu+\frac{\mu_t}{\sigma_\kappa}\right)\frac{\partial \kappa}{\partial x_j}\right]+G_\kappa+G_b-\rho\varepsilon-Y_M+S_\kappa \tag{4}$$

$$\frac{\partial}{\partial t}(\rho\epsilon)+\frac{\partial}{\partial x_j}(\rho\varepsilon u_j)=\frac{\partial}{\partial x_j}\left[\left(\mu+\frac{\mu_t}{\sigma_\varepsilon}\right)\frac{\partial \varepsilon}{\partial x_j}\right]+\rho C_1 S_\varepsilon-\rho C_2\frac{\varepsilon^2}{\kappa+\sqrt{\nu\varepsilon}}+C_{1\varepsilon}\frac{\varepsilon}{\kappa}C_{3\varepsilon}G_b+S_\varepsilon \tag{5}$$

where;

$$C_1=max\left[0.43,\frac{\eta}{\eta+5}\right],\eta=S\frac{\kappa}{\varepsilon},S=\sqrt{2S_{ij}S_{ij}}$$

in these equations, G_κ is the kinetic energy of turbulence due to mean velocity gradients, G_b the turbulence kinetic energy due to the buoyancy, Y_M the contribution of fluctuating expansion to the overall dissipation rate in compressible turbulence (negligible in liquids), $C_{1\varepsilon}$, C_2, and $C_{3\varepsilon}$ constants, σ_κ, σ_ε the κ and ε for turbulent Prandtl numbers, respectively. S_κ and S_ε are user-defined source terms.

3. Computational model of Dynamic mesh structure

Dynamic meshing can be used to simulate the range of displacements or boundary condition degradation resulting from a time-dependent flow field. This technology provides three distinct models: layering, arc smoothing, and local remeshing. Since triangular mesh structures are preferred in this study, two arc smoothing and new mesh models are developed to renew the mesh structures when elliptical gears rotate. Equation (6) [20] represents the general formula for the dynamic network structure computation model.

$$\frac{d}{dt}\int_V \rho\varphi dV+\int_{\partial V}\rho\varphi\left(\vec{u}-\vec{u}_s\right)d\vec{A}=\int_{\partial V}\Gamma\nabla\varphi d\vec{A}+\int_V S_\varphi dV \tag{6}$$

in this equation, $\vec{u}$ is the fluid velocity vector, $\vec{u}_s$ deformation speed of the dynamic mesh, Γ the diffusion coefficient, S_φ φ′s the source fluid, and ∂V the volume boundary.

4. Material and methods

In this study, the experimentally measured flow rates from flow meters designed and manufactured based on three different a/b ratios, three different modules, and three different tooth numbers were contrasted with the flow rates derived from CFD analysis. In accordance with the Taguchi L_9 experiment set, nine different flowmeters with varied parameters were manufactured, and CFD models were created. ANSYS Fluent was used for running a flow analysis on the CFD models. The Taguchi L_9 levels and factors are displayed in Table 1, and the manufactured flowmeters and CFD models are shown in Table 2.

Table 1
Taguchi L_9 levels and factors of elliptical gear parameters.

	Factors		
	a/b ratio (A)	m (module) (B)	z (number of teeth) (C)
1st Level (1)	1,25	1,60	25,00
2nd Level (2)	1,40	2,00	32,00
3rd Level (3)	1,60	2,50	40,00

Table 2
Elliptical gear and flowmeter designs according to Taguchi L_9.

	Flowmeter Code								
	Db-01	Db-02	Db-03	Db-04	Db-05	Db-06	Db-07	Db-08	Db-09
Factor A	1	1	1	2	2	2	3	3	3
Factor B	1	2	3	1	2	3	1	2	3
Factor C	1	2	3	2	3	1	3	1	2

The mathematical equations and terminology on elliptical gear design may be described as follows: ellipse is used to denote the shape surrounding the surfaces resulting from the intersection of cylinders or cones at an inclined angle to the base plane. The distances between the focus points of an ellipse are constant and equivalent to the length of the primary axis. The coordinates of these points are referred to as elliptic coordinates (Fig. 1), and the polar equations of elliptic curves may be derived using the following equations [13,22].

According to Fig. 1, the equations are as follows.

$$r_1 = \frac{P}{1 - e.\cos(\theta_1)}, P, e \in R \tag{7}$$

where, R and e are real numbers. e is the eccentricity of the ellipse and is calculated by Equation (8).

$$e = \frac{\sqrt{a^2 - b^2}}{a} \tag{8}$$

The focal point c_0 of the ellipse is found by Equation (9).

$$c_0 = \sqrt{a^2 - b^2} \tag{9}$$

where, a is the large radius of the ellipse and b is the small radius of the ellipse.

In other words, the P value can be calculated by Equation (10).

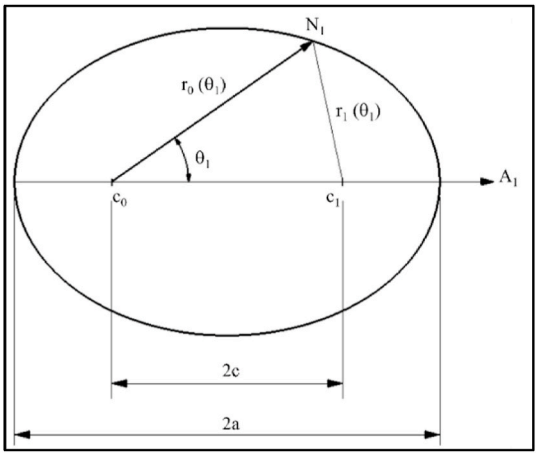


Fig. 1. $\overline{c_0N_1}$ position vector and $\overline{c_0A_1}$ polar axis.

$$P = a.(1 - e^2) \tag{10}$$

Rolling a rack-shaped cutter on a section ellipse without sliding produces elliptical gearing. The rack comprises two angularly symmetrical lines that constitute the pressure angle (α) of the cutter concerning the two-dimensional coordinate system, and the cutter's coordinates are derived using complex numbers (Fig. 2).where, $i^2 = -1$ and the step line of the cutter coincides with the complex axis. The complex coordinates of the sth corner points of the cutter are given below.

$$t_s = t_{s-4} + i.m.\pi \tag{12}$$

s = 4,5, ... … 4z-1 and z = z+1 is the total number of teeth of the rack cutter. Complex coordinates of the sth corner of the step line.

$$r_M = (t_s - i.L).e^{(i\mu)} + X + i.Y - c_0 \tag{13}$$

where, L is the circumference of the step ellipse and is calculated by the following equation.

$$L = \int_0^{2\pi} \sqrt{r^2 + \left(\frac{\partial r}{\partial \theta}\right)^2} d\theta = m.\pi.z \tag{14}$$

$$X = r.\cos(\theta) \tag{15}$$

$$Y = r.\sin(\theta) \tag{16}$$

and the slope of the line tangent to the step ellipse.

$$\mu = \frac{\pi}{N} \tag{17}$$

The design of elliptical gears included considering the equations mentioned earlier. A rack-shaped cutter with a clutch angle 20° was developed using a macro program within the Catia V5 environment, using the rolling technique on the pitch ellipse as seen in Fig. 3.

Elliptical gear pairs were ground in St37 material on Prompt SG-4080AH plane grinding machine with a gear width of 20 mm. The chemical and mechanical properties of the materials used are given in Tables 3 and 4, respectively. Two-dimensional drawings of the elliptical gear pairs were taken, transferred to the Computer Aided Manufacturing (CAM) environment, G codes were produced for the CNC wire erosion machine and cut and manufactured on Accutex Al-600 SA brand CNC electrical discharge machine. The 3D models of the flowmeter bodies were transferred to the CAM environment, G codes were generated for first roughing and then fine machining operations and manufactured from aluminum 6061 series on Hartford Pro 1000 CNC VMC branded CNC milling machine.

The fluid inlet and outlet diameters of the flowmeter bodies were drilled as 14.5 mm and 1/2″ taps were drawn. A gasket channel was opened in the flowmeter cover and sealing was ensured with a 4 mm diameter gasket. A neodymium magnet was placed on the rotor gear by drilling a magnet cavity. A microcontroller circuit with a magnetic field sensor was developed to measure the speed of the rotor gear of the flowmeters, and the flowmeter assembly is shown in Fig. 4.

A 9V battery powered this circuit; the magnetic field sensor was triggered at each rotation of the rotor gear; and the Revolutions Per Minute (RPM) (.) of the rotor gear was calculated by measuring the time between the two triggers. The data obtained from RPM and flow rates were displayed and recorded on the 0.96″ OLED display. The flow rates are shown in Table 5, while the RPM is in Table 6.

On the experimental apparatus depicted in Fig. 5, the manufactured flowmeters are calibrated using a reference analog flowmeter. The reference analog flowmeter is a turbine type flowmeter that meets the requirements of ISO 2715:2017. Flow experiments were conducted on the flowmeters at five distinct pressure levels: 2.5 MPa, 3.0 MPa, 3.5 MPa, 4.0 MPa, and 4.5 MPa with the pressure gauge manually adjusted. Nevertheless, the hydraulic system was driven by a gear pump with a

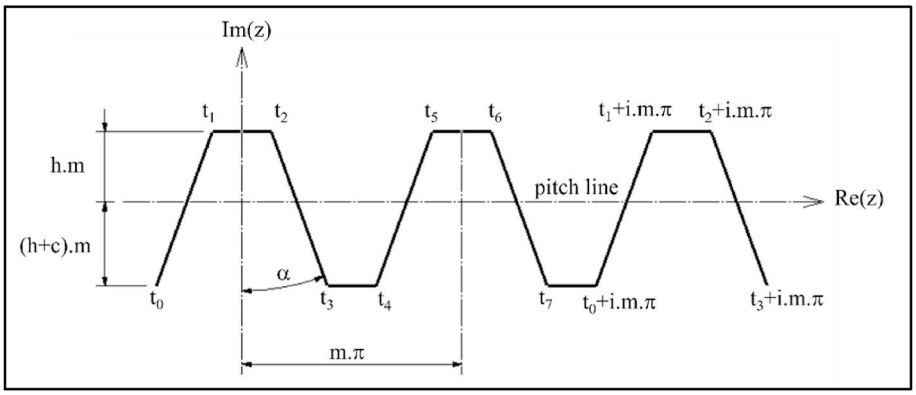


Fig. 2. 2D model of the rack cutter.

$$\left.\begin{aligned} t_0 &= m.\left[h_1 - i.\left(\frac{\pi}{4} + h_1.\tan(\alpha)\right)\right] \\ t_1 &= m.\left[-h_2 - i.\left(\frac{\pi}{4} - h_2.\tan(\alpha)\right)\right] \\ t_2 &= m.\left[-h_2 + i.\left(\frac{\pi}{4} - h_2.\tan(\alpha)\right)\right] \\ t_3 &= m.\left[h_1 + i.\left(\frac{\pi}{4} - h_2.\tan(\alpha)\right)\right] \end{aligned}\right\} \tag{11}$$

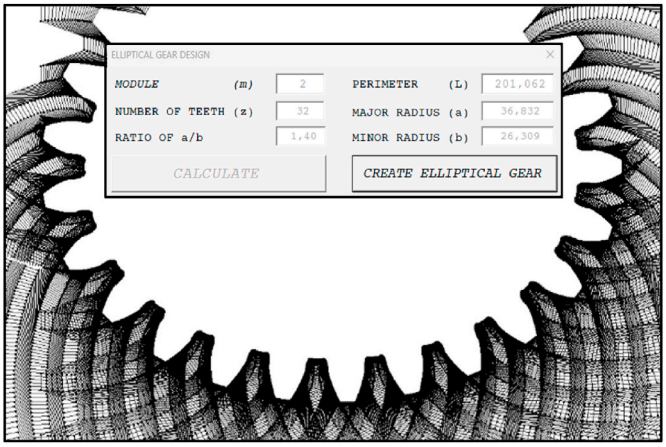


Fig. 3. Creation of tooth profiles based on the rolling method with macro program.

flow rate of 50 L/min, a maximal pressure of 27 MPa, and No. 46 oil. Flow experiments were conducted at temperatures between 40 °C and 45 °C. This oil has an 872 kg/m^3 density and a kinematic viscosity of 46 cSt at 40 °C (Shell Tellus S2 V46).

The dynamic mesh calculates the flow rates obtained from the CFD analysis of the flowmeters. In Equation (18), the radius corresponding to the rotation angle of the pitch ellipses of elliptical gears [25] is parametrically defined.

$$r_1(\theta_1) = \frac{2 \bullet a \bullet b}{(a+b) - (a-b) \bullet \cos(2\theta_1)}, (mm) \tag{18}$$

The transmission between elliptical gear pairs is shown in Fig. 6. In Fig. 6, the left-hand gear is the rotor, and the right-hand gear is the rotating gear. a is the major radius of the step ellipse; b is the minor radius of the pitch ellipse; θ_1 is the rotation angle of the rotor gear; θ_2 is the rotation angle of the rotating gear; r_1 is the radius of the rotor gear depending on the angle θ_1; r_2 is the radius of the rotating gear depending on the angle θ_2; E is the inter-axis distance of gears; ω_1 is the angular speed of the rotor gear; and ω_2 is the angular velocity of the rotating gear.

The angular speed of the rotor gears is calculated using Equation (19) based on the RPM values read from the manufactured flow meters, and Equation (20) is used to calculate the cycle ratio between the elliptical gears. It is defined as:

$$\omega_1 = \frac{2\pi}{60}.RPM, \left(\frac{rad}{s}\right) \tag{19}$$

$$\omega_1.r_1 = \omega_2.r_2 \tag{20}$$

where;

$$r_2 = E - r_1, (mm) \; ve \;\; E = a + b, (mm)$$

The instantaneous radius change of the rotor gear with time is given

Table 4
Mechanical properties of St37 material and Al6061 [23,24].

Material	Mechanical properties		
	Yield Strength (MPa)	Tensile Strength (MPa)	Strain (%)
St37	235	350–480	25
Al 6061	240–275	260–310	8–12

Table 3
Chemical compounds of St37and Al6061 material [23,24].

	Chemical compounds (%)											
Material	C	Fe	P	S	Mn	Si	Cu	N	Mg	Zn	Ti	Cr
St37	0,17	98,031	0,045	0045	1,4	0,3		0,009				
Al 6061		0,7			0,15	0,4-0,8	0,6-1,1		0,8-1,2	0,25	0,15	0,04-0,35

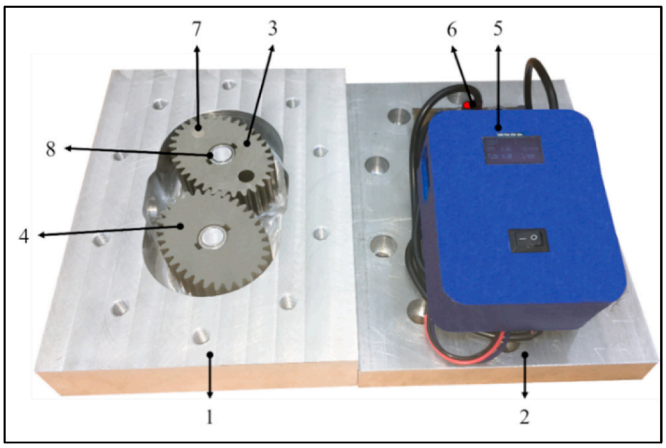


Fig. 4. Flowmeter assembly. 1 - Body, 2 - Cover, 3 - Rotor gear, 4 - Elliptical gear, 5 - Electronic circuit box, 6 - Magnetic field sensor, 7 - Neodymium magnet, and 8 - HK1012 needle bearing.

in Equation (21). In this equation, t refers to time.

$$r_1 = \frac{2 \bullet a \bullet b}{(a+b) - (a-b) \bullet \cos(2\omega_1 t)}, (mm) \tag{21}$$

when pressurized fluid reaches the rotor gear of manufactured flowmeters, the gear starts to rotate. Under the cycle ratio, this rotational motion rotates the rotating gear. This rotation ratio was applied to CFD models with User-Defined Functions (UDF) in the ANSYS Fluent environment (Fig. 7).

In the CFD models of nine different flow meters (Fig. 8), fluid inlet velocity and pressure values corresponding to five different pressure values keen for each flow meter were designated as fluid inlet boundary conditions. Five pressure values were set as fluid outlet boundary conditions to generate flow analysis results. Table 7 shows the number of nodes and elements in CFD mesh models. CFD flow analyses were performed on a computer with an Intel Core 7–12700 processor, 16 GB of memory, and an NVIDIA GeForce RTX 3050 graphics card, and each CFD analysis took approximately 12 h. Fig. 9a depicts the circuit diagram of experimental equipment used to ascertain the flow rates measured by the manufactured flowmeters. As shown in Fig. 9b, the allocation of pressure values as the output boundary condition signifies that performance tests of the manufactured flowmeters are conducted under pressure. Fluid inlet velocities are calculated by Equation (22). The Realizable κ - ε turbulence model was chosen as the turbulent flow model, and the coupled algorithm was selected as the solver. The reason for choosing this solver is that it can solve momentum and pressure-based continuity equations together.

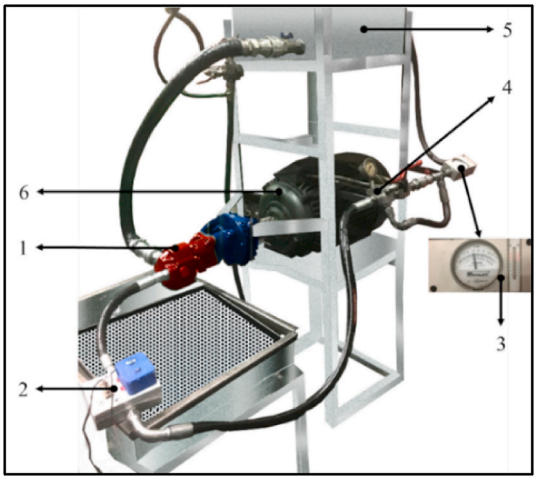


Fig. 5. Flow test setup. 1 - Gear pump, 2 - Manufactured flowmeter, 3 - Reference analog flowmeter, 4 - Pressure control valve, 5 - Tank, and 6 - Electric motor.

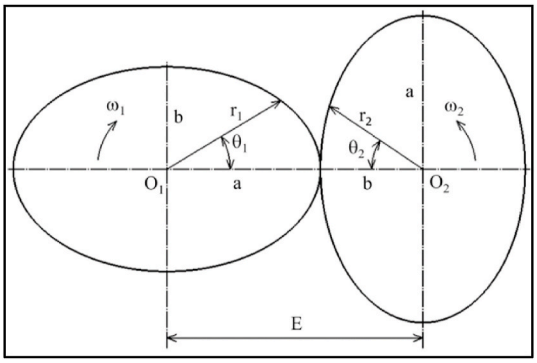


Fig. 6. Transmission scheme of elliptical gear pairs.

Table 5
Measured flow rates (m^3/s).

		Flowmeter Code								
		Db-01	Db-02	Db-03	Db-04	Db-05	Db-06	Db-07	Db-08	Db-09
Pressure (Mpa)	**2,50**	6,7E-04	7,5E-04	7,5E-04	7,0E-04	7,5E-04	7,7E-04	7,0E-04	7,0E-04	7,6E-04
	3,00	6,6E-04	7,5E-04	7,5E-04	6,9E-04	7,5E-04	7,6E-04	7,0E-04	6,9E-04	7,5E-04
	3,50	6,6E-04	7,4E-04	7,5E-04	6,9E-04	7,5E-04	7,5E-04	6,9E-04	6,9E-04	7,5E-04
	4,00	6,6E-04	7,4E-04	7,4E-04	6,9E-04	7,4E-04	7,5E-04	6,9E-04	6,8E-04	7,4E-04
	4,50	6,6E-04	7,3E-04	7,4E-04	6,8E-04	7,4E-04	7,4E-04	6,9E-04	6,7E-04	7,4E-04

Table 6
Measured rotor gear speed (RPM).

		Flowmeter Code								
		Db-01	Db-02	Db-03	Db-04	Db-05	Db-06	Db-07	Db-08	Db-09
Pressure (MPa)	**2,50**	1920	930	419	1040	485	700	550	780	356
	3,00	1911	926	418	1032	483	694	548	772	354
	3,50	1908	922	417	1027	482	687	546	765	351
	4,00	1900	917	415	1020	480	684	545	759	348
	4,50	1896	910	412	1015	477	678	543	752	347

```
#include "udf.h"

#define RPM 1920 //  rev/min
#define W (2*3.141592*RPM)/60 // rad/s

DEFINE_CG_MOTION(gear1_motion,dt,vel,omega,time,dtime)
{
omega[2] = W; // angular velocity of the rotor gear.
}
DEFINE_CG_MOTION(gear2_motion, dt, vel, omega, time, dtime)
{
double a = 22.08707;// major radius of the pitch ellipse.
double b = 17.669656;// minor radius of the pitch ellipse.
double r1, r2, ratio;

r1 = (2 * a * b) / ((a + b) - (a - b) * cos(2 * W * time)); // instantaneous time-dependent radius of the rotor gear.
r2 = a + b - r1; // instantaneous time-dependent radius of the rotating gear.
ratio = r1 / r2; // the cycle ratio of elliptical gears.

omega[2] = -W * ratio; // angular speed of the rotating gear.
}
```

Fig. 7. Time-dependent UDF code of the cycle ratio of elliptical gear pairs.

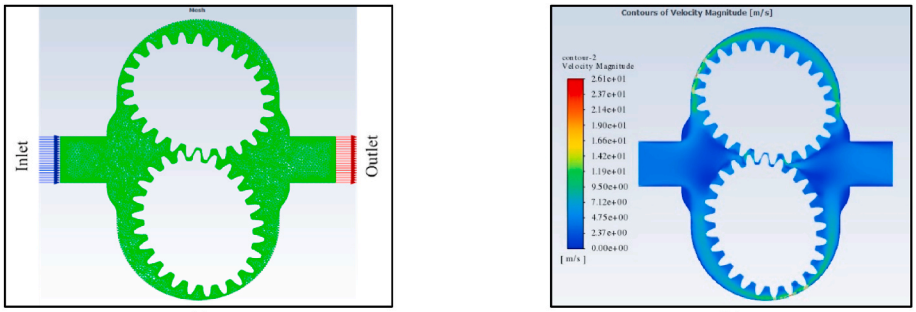


Fig. 8. a) Mesh structure of CFD models. b) CFD analysis inlet and outlet velocity results.

Table 7
Number of nodes and elements of the mesh structure of CFD models.

	Flowmeter Code								
	Db-01	Db-02	Db-03	Db-04	Db-05	Db-06	Db-07	Db-08	Db-09
Nodes	31280	49841	80825	40369	65537	50682	52404	40486	68483
Elements	56883	90829	148079	73530	120216	92737	95974	73957	126137

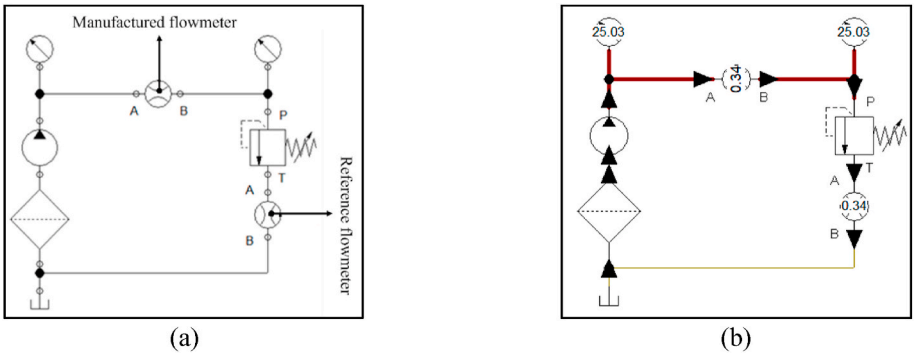


Fig. 9. a) Circuit diagram of the experimental set. b) Inlet and outlet pressures of the manufactured flow meter.

$$Q = V.A, \left(\frac{m^3}{s}\right) \tag{22}$$

where V is the inlet velocity of the fluid, A is the inlet area of the fluid.

5. Results and discussion

The flow rates obtained experimentally from the flowmeters manufactured according to the Taguchi L9 test setup and the flow rates obtained from the analysis results of the CFD models of the manufactured flow meters decreased as the pressure increased. On the other hand, the average change of the flow rates obtained from all manufactured and

CFD models was −0.0102 %.

Examining the flow meters with a modulus of m = 1.60 (Fig. 10) establishes an average difference of −0.017 % between the flow rates measured by the Db-01 flowmeter and those calculated via the CFD analysis. Similarly, the average flow rate change for the flowmeters designated Db-04 and Db-07 was −0.008 % and −0.012 %, respectively. The largest percentage change in flow rates was found to be −0.0750 % at 4.50 MPa pressure, and the smallest percentage change was established to be −0.0060 % at 4.00 MPa pressure for the flowmeter with the code Db-01.

When the flow meters with modulus m = 2.00 are considered as shown in Fig. 11, the average variation between the measured and CFD-analyzed flow values is −0.015 % for the flow meter coded Db-08, -0.017 % for the flow meter coded Db-02, and -0.016 % for the flow meter coded Db-05. On the other hand, it was seen that the flow meter coded Db-05 had the maximum percentage change at 4.00 MPa pressure with −0.0788 %, while the flow meter coded Db-02 had the slightest percentage change at 4.50 MPa pressure with 0.0002 %.

Fig. 12 demonstrates the average differences between CFD and measured flow rates for flow meters with the parameter m = 2.50. The average flow rate variation for flow meters Db-06, Db-09, and Db-03 was 0.004 %, −0.015 %, and 0.005 %, respectively. In addition, it was found that the percentage flow rate change at 3.00 MPa pressure with the flow meter designated Db-03 was the highest with a value of 0.0855 %, and the lowest with a value of −0.0024%at 3.50 MPa pressure. Considering the average variations in flow rate between the measured flow rates and the flow rates derived from CFD analysis in all flow meters, it was determined that the CFD model was compatible with the manufactured flow meters.

Table 8 shows the percentage variations in flow rates resulting from CFD analysis. The flow meter coded as Db-03 displayed the largest percentage change at 0.0855 % under 3.00 MPa pressure, while the flow meter coded as Db-02 revealed the slightest percentage change at 0.0002 % at 4.50 MPa pressure.

According to the CFD analysis, the determination of an enormous percentage change with the flow meter coded Db-03 can be explained as follows: internal leaks occurring in the flow tests of the manufactured flow meters in the experimental environment, the formation of friction with the flow meter body during the rotation of the elliptical gears under pressure and the mass moments of inertia of the elliptical gears were ignored in the 2D CFD analysis. In addition, the evolvent tooth profiles of the elliptical gear pairs of the manufactured flowmeters actually work by contacting each other, but since the dynamic network structure is used in the CFD analysis and the mesh is re-mesh according to the

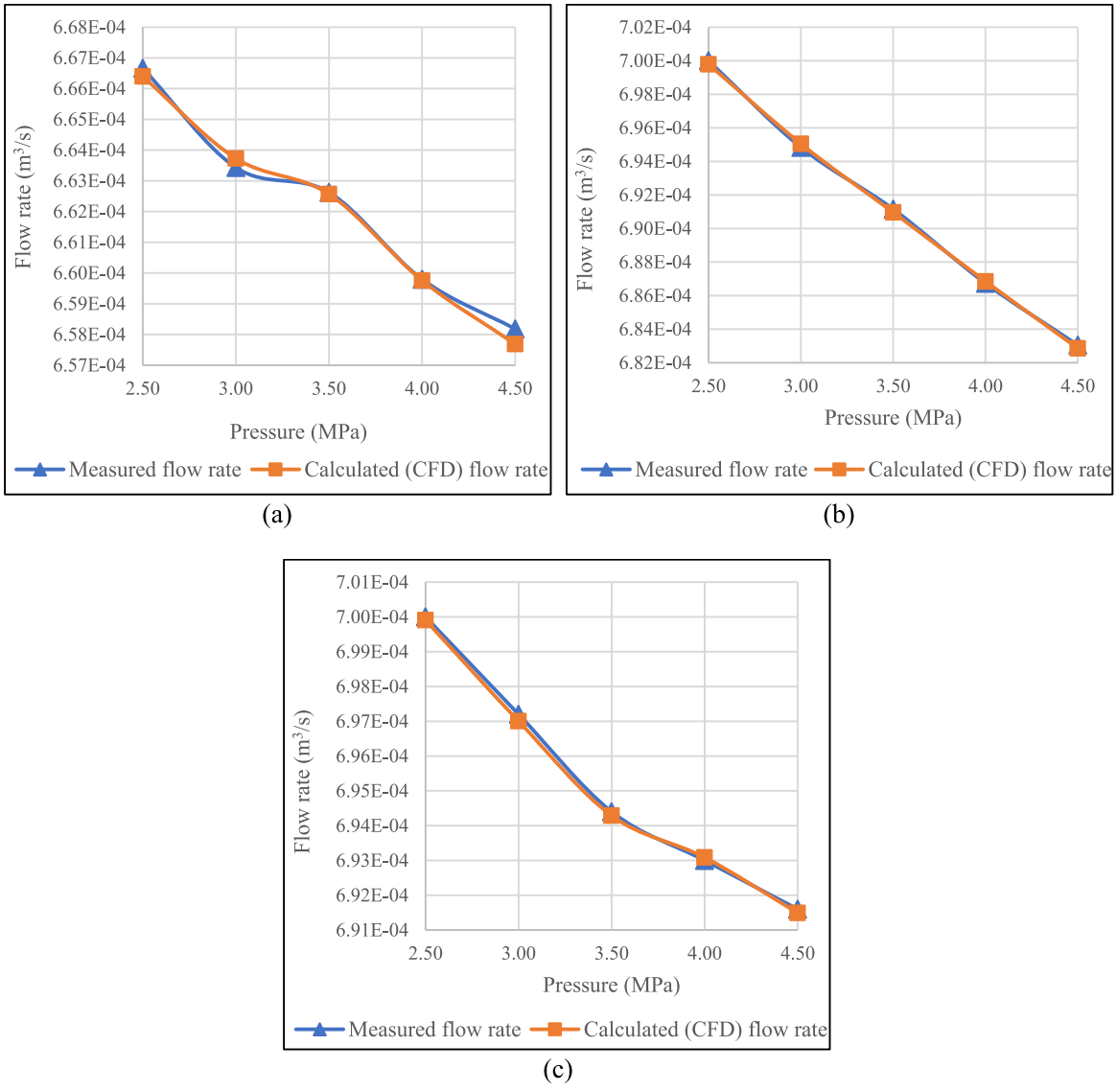


Fig. 10. Comparison of measured - CFD flow rate versus pressure for flow meters with parameter m = 1.60. a) Db-01 b) Db-04 c) Db-07.

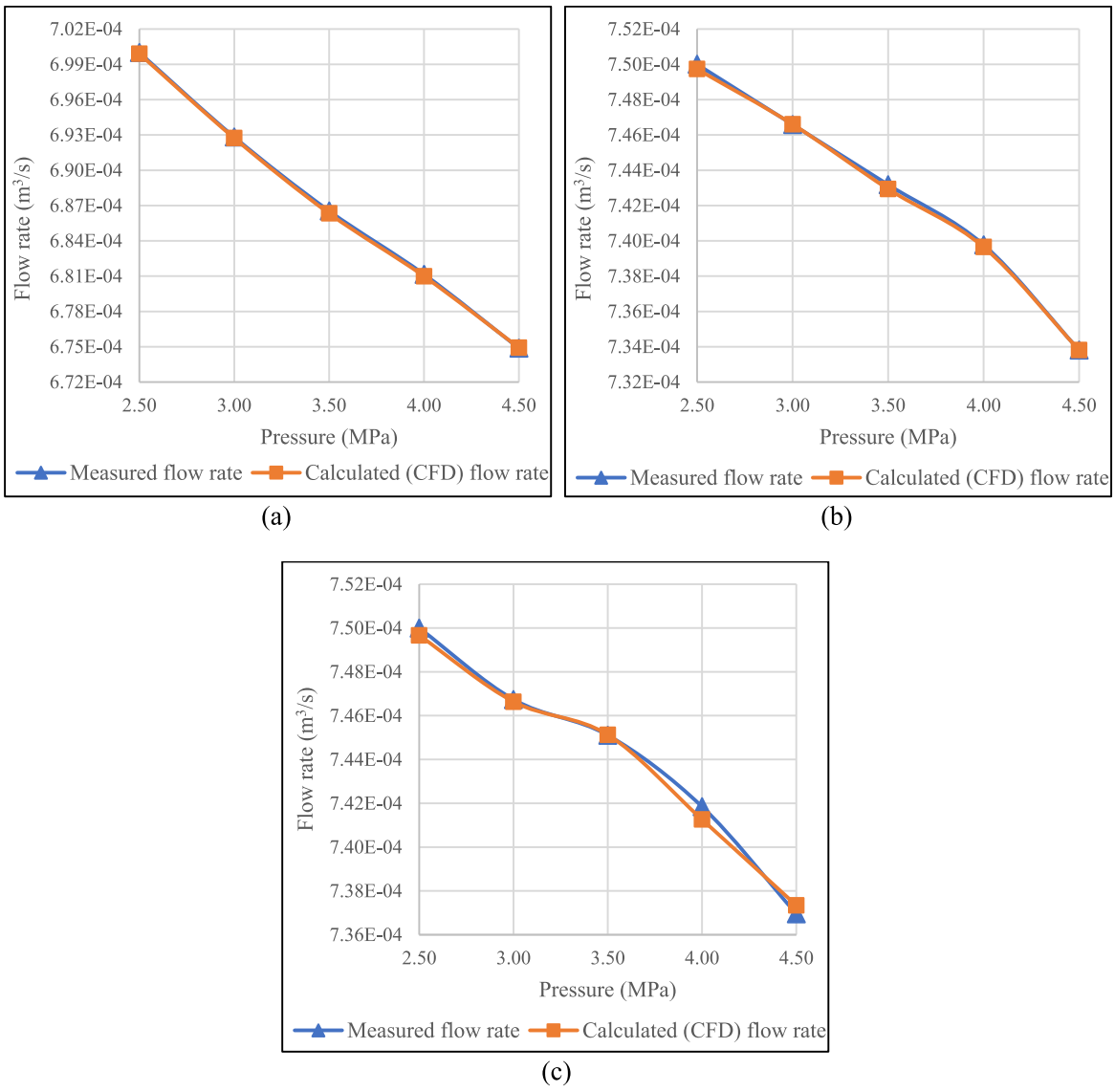


Fig. 11. Comparison of measured - CFD flow rate versus pressure for flow meters with parameter m = 2.00. a) Db-08 b) Db-02 c) Db-05.

displacements calculated by the time-dependent UDF code, accordingly, if the evolvent profiles of the elliptical gear pairs defined in the CFD analysis are in contact with each other, the inability to form a mesh in the analysis occurs. To prevent these meshing defects in the CFD model, it is necessary to diminish the tooth involute of the elliptical gears by offsetting (Fig. 13a). The dynamic mesh structure can be reconstructed, and CFD analysis can be conducted in this situation. This is not an accurate representation of the actual flow meter operation and causes errors in the calculated flow rates. The circumstance between the flow meter body and the elliptical gear is analogous. To re-mesh the dynamic network, sufficient clearance between the flow meter body and the elliptical gear must be provided in the CFD model (Fig. 13b). These distances are specified as 0.15 mm in CFD models. The time required to reconstruct a time-dependent, dynamic network increases as the gap size decreases. In the CFD analysis, the selection of turbulent flow is also a problem. The irregularity of the turbulent flow creates a difference between the flow rate acquired by the experiment and the flow rate calculated by CFD analysis.

When analyzing the internal flow characteristics of the CFD models of the flowmeters, it is observed that the velocity vectors of the fluid conveyed in the tooth cavities are perpendicular to the tooth evolvent profiles of the elliptical gears (Fig. 14a). Where the elliptical gears begin to engage (Fig. 14b) and where the engagement ends (Fig. 14c), larger velocity vectors are formed opposite to the vectors formed in the tooth cavities. These velocity vectors attempt to prevent the elliptical gears from rotating and causing turbulence in that region. The velocity vector reaches its maximal value where the flow meter body and the tooth apex of the elliptical gear are closest together (Fig. 14d), resulting in pressure loss in that region. Since there is a sudden cross-sectional contraction in the region closest to the flowmeter body and elliptical gear, and it has the smallest cross-section, it is natural, according to the Bernoulli principle, that the flow velocity provided by the pump reaches its highest value in this region. In reality, this cross-section is smaller, and there is a discrepancy between the flow rates measured by manufactured flow meters and those calculated by CFD analysis.

Between the elliptical gear and the body wall, the fluid is gathered speed, and directed toward the outflow of the flow meter. In light of these explanations, when the elliptical gear parameters are considered, the modulus value is the most significant parameter affecting the tooth gap. As the modulus value increases, the composite of the velocity vectors on the involute curve increases. In response to this composite velocity, with the flow rate provided by the pump to the flow meter, greater velocities than the composite velocity of the fluid in the tooth gap are formed in the opposite direction. In this case, the fluid creates

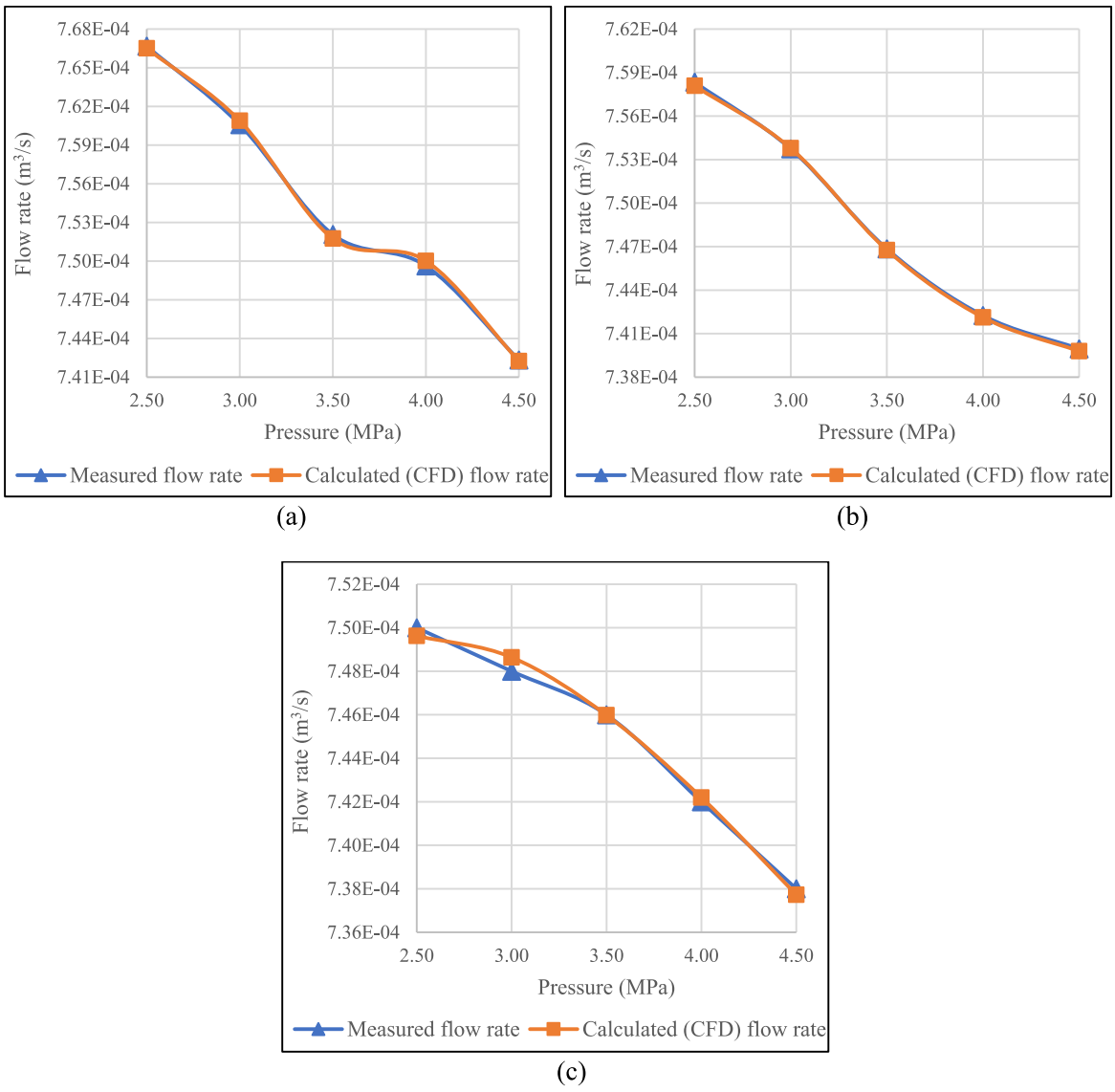


Fig. 12. Comparison of measured - CFD flow rate versus pressure for flow meters with parameter m = 2.50. a) Db-06 b) Db-09 c) Db-03.

Table 8
changes (%) of the flow rates manufactured and obtained from CFD analysis.

		Flowmeter Code								
		Db-01	Db-02	Db-03	Db-04	Db-05	Db-06	Db-07	Db-08	Db-09
Pressure (MPa)	**2,50**	−0,0401	−0,0358	−0,0498	−0,0298	−0,0446	−0,0203	−0,0134	−0,0147	−0,0320
	3,00	0,0446	0,0015	0,0855	0,0297	−0,0135	0,0396	−0,0281	−0,0131	0,0065
	3,50	−0,0083	−0,0327	−0,0024	−0,0280	0,0026	−0,0418	−0,0160	−0,0300	−0,0107
	4,00	−0,0060	−0,0167	0,0265	0,0167	−0,0788	0,0518	0,0125	−0,0241	−0,0172
	4,50	−0,0750	0,0002	−0,0367	−0,0281	0,0523	−0,0109	−0,0156	0,0065	−0,0213

larger turbulences in the engagement and disengagement zones of the elliptical gears, causing an increase in internal leakage, slowing down the rotation speed of the gears, and affecting the flow measurement accuracy. Changing the number of teeth of elliptical gears changes the area of the engagement and disengagement zone of the gears, causing turbulence to change in those regions. On the other hand, an increase or decrease in the a/b ratio changes the area of the flow chamber of the flow meter. Thus, the velocity of the fluid in the flow chamber also changed. As the a/b ratio increased, the flow velocity from the elliptical gear to the flow meter body decreased (Fig. 15).

The number of experiments and manufacturing costs for flow meters are reduced using the Taguchi method. Since pressure variables do not affect the flow meter's expense, they were not evaluated in the Taguchi analysis. The Taguchi method was applied to the results of the CFD analysis. According to the Signal-to-Noise ratio (S/N) obtained in the largest best case according to the flow rates (Fig. 16), it was determined that the most suitable elliptical gear parameters a/b = 1.40, m = 2.50 mm, and z = 40 teeth, as well as a/b = 1.40, m = 2.50 mm and z = 32 teeth parameters, are primarily preferable for elliptical spur gear design and manufacturing.

According to the results of the multi-way analysis of variance (Table 9), which was performed by considering all parameters (a/b, m,

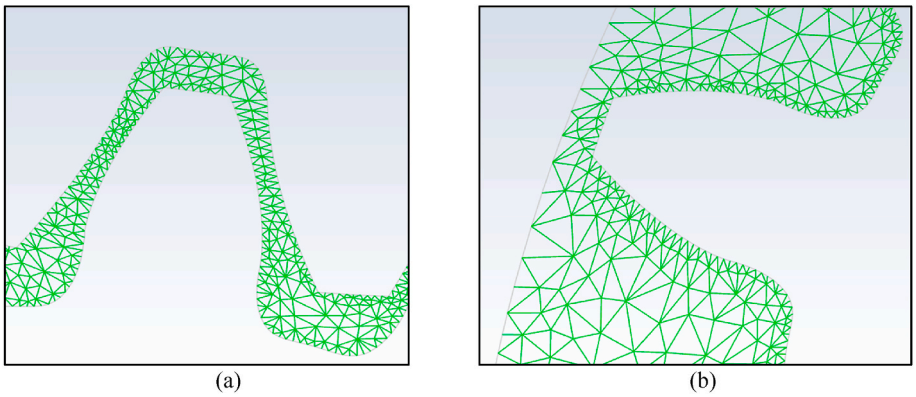


Fig. 13. a) Mesh structure of tooth gaps of elliptical gears. b) Mesh structure of elliptical gear - flow meter body gaps.

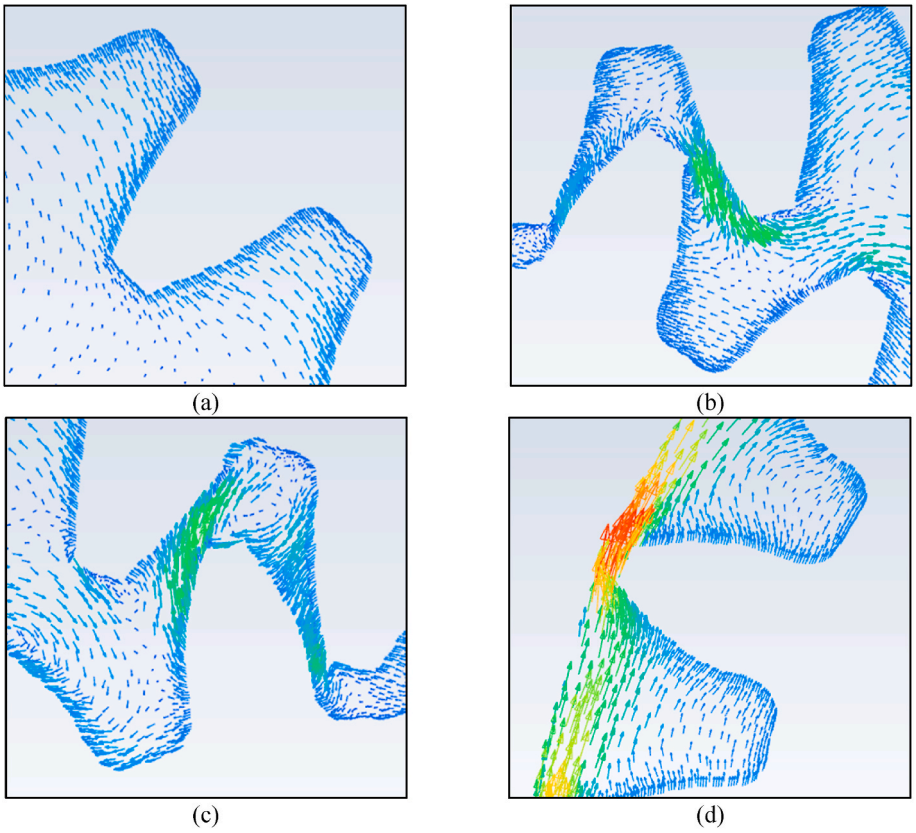


Fig. 14. a) Velocity vector at the tooth gap. b) Velocity vector and turbulence at the beginning of engagement. c) Velocity vector and turbulence at the end of engagement. d) Velocity vector between the gear and the body wall.

z, pressure) that are effective on the CFD models at a 95 % confidence interval, the modulus value was the most influential variable according to the contribution rate with 65.25 %; the number of teeth was the second most important parameter with 10.52 %; and the a/b ratio was the least effective variable with 0.96 %. Considering the interactions between the a/b ratio, modulus, number of teeth, and pressure variables, it was determined that m*z contributed the most with 17.25 %, and a/b*Pressure contributed the least with 0.05 %. When the regression values of the CFD-calculated flow rates were analyzed, it was seen that R^2 = 99.00 % and R^2 (corrected) = 98.71 % suggest a trend very close to a linear relationship and are trustworthy. Because it is the only parameter used to compute gears' pitch and tooth height, it is natural that the module value has the most significant impact on the calculated flow rates.

As the module value increases, a gear's pitch and tooth height increase, while a decrease in the module value reduces pitch and tooth height. Increasing the pitch and tooth height increases the fluid transported through a tooth gap. Similarly, increasing the number of teeth parameter, which provides the second greatest contribution, results in the same number of tooth gaps as teeth, thereby increasing the quantity of fluid transported in the tooth gaps and the flow rate. Analyzing the binary interactions of the parameters reveals that m*z has the highest contribution rate at 17.28 %, while a/b*pressure has the lowest contribution rate at 0.05 %. The contribution rate is highest for m*z, as m*z is a parameter that affects both the circumference of the pitch circle in gear wheels and the circumference of the pitch ellipse in elliptical gears.

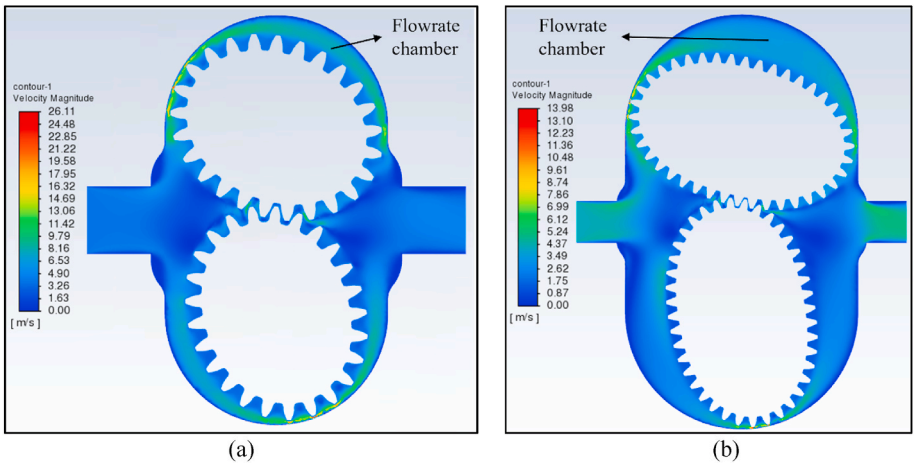


Fig. 15. 2.5 MPa pressure. a) m = 1.60 z = 25 a/b = 1.25 elliptical gear speed analysis. b) m = 1.60 z = 40 a/b = 1.60 elliptical gear speed analysis.

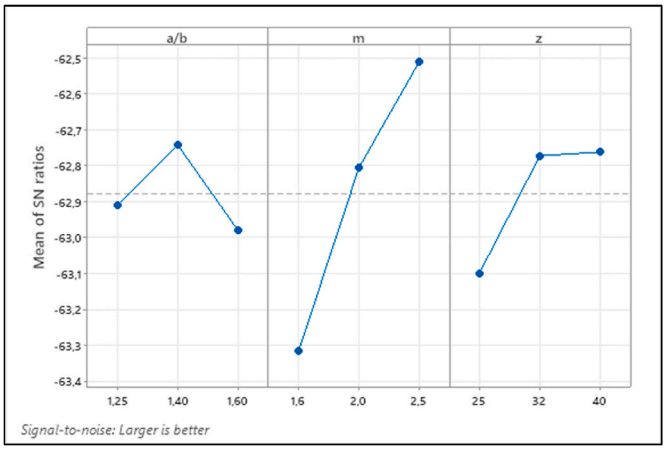


Fig. 16. S/N ratio of the Taguchi L9 experimental set largest-best analysis according to CFD analysis results.

6. Results

In this study, it is aimed to optimize elliptical gear flowmeters and to verify the flow rates measured by the flowmeters manufactured within the scope of the study with CFD analysis. Manufactured flowmeters; Uyar Hidrolik San. Tic. Ltd. (www.uyarhidrolik.com) company, used to determine the flow rates produced by commercially manufactured pumps and has a reference flowmeter, was calibrated in a test setup. Then, the flow rates measured with the manufactured flowmeters and the speeds of the rotor gears were measured and used as boundary conditions in CFD analysis.

As the fluid pressure of the flowmeters manufactured and CFD analyzed according to the Taguchi L9 test set increases, the measured and CFD analyzed flow rates decrease, and the average percentage change in flow rate is −0.0102 %, indicating that the manufactured flowmeters and CFD models are compatible. Nevertheless, both the CFD calculated and measured flow rates was very close to each other with a mean change of −0.0102 % and the CFD calculated flow rates are reliable with R^2 = 99.00 %, indicating that the internal cavities of the flow meters are properly manufactured and well-sealed.

Considering the necessity of recalculating the time-dependent dynamic mesh structure in CFD models, the elliptical gear pairs, which are in contact in reality, were prepared in CFD models without contacting each other and with a gap between them. A similar situation was realized by giving more space between the elliptical gear and the flowmeter body wall than it should be in reality. In addition, frictions between the elliptical gear pairs and the flow meter body, gear moments of inertia, and internal leakages in the experimental environment were ignored in the CFD analysis. For these reasons, it is concluded that there are differences between the flow rates obtained experimentally and the flow rates calculated by CFD analysis.

According to the internal flow characteristics obtained from the CFD analysis of elliptical gear flowmeters, the velocity vector of the fluid carried in the tooth cavity acts perpendicular to the tooth involute profile, and it is determined that in the regions where the elliptical gears engage, and disengage, the velocity vectors in the tooth cavities act in

Table 9
Analysis of variance according to CFD analysis results.

Source	DF	Seq SS	Contribution	Adj SS	Adj MS	F-Value	P-Value
Regression	10	0,000000	99,00 %	0,000000	0,000000	336,96	0,000000
a/b	1	0,000000	0,96 %	0,000000	0,000000	36,86	0,000001
m	1	0,000000	65,25 %	0,000000	0,000000	4,30	0,045691
z	1	0,000000	10,52 %	0,000000	0,000000	296,67	0,000000
Pressure	1	0,000000	2,80 %	0,000000	0,000000	0,02	0,895482
a/b*m	1	0,000000	0,65 %	0,000000	0,000000	241,77	0,000000
a/b*z	1	0,000000	1,28 %	0,000000	0,000000	115,02	0,000000
a/b*Pressure	1	0,000000	0,05 %	0,000000	0,000000	1,67	0,204560
m*z	1	0,000000	17,28 %	0,000000	0,000000	588,20	0,000000
m*Pressure	1	0,000000	0,09 %	0,000000	0,000000	3,12	0,086124
z*Pressure	1	0,000000	0,13 %	0,000000	0,000000	4,45	0,042421
Error	34	0,000000	1,00 %	0,000000	0,000000		
Total	44	0,000000	100,00 %				

DF: Degrees of freedom, Seq SS: Ordered sum of squares, Adj SS: Adjusted sum of squares, Adj MS: Adjusted mean squares.
R^2 = %99,00 R^2 (adjusted) = %98,71.

the opposite direction and at a higher velocity. These reverse velocity vectors cause turbulence in the regions where the gears engage and disengage, preventing the elliptical gear from rotating and causing internal leakage and flow calculation errors. In addition, it was determined that the regions of elliptical gear flowmeters where the gear and the flowmeter body are closest to one another have the maximum velocity values. According to Bernoulli's principle, it is natural that the velocity reaches its maximum value in this region. In reality, this cross-section is smaller, and it has been determined that there is a difference between the flow rates measured by the manufactured flow meters and those computed by CFD analysis.

Since a change in the modulus value, which is one of the elliptical gear design parameters, causes a change in the amount of fluid carried in the tooth cavities, it was concluded that it would alter the composite velocity vector on the tooth involute profile and the velocity vector acting in the opposite direction, thereby affecting turbulence, internal leakage, and rotational speed of the elliptical gear. Thus, it has been determined that it causes errors in the results of CFD analyses. Changing the number of teeth on elliptical gears affects turbulence formation and internal leakage, impacting the gears' engagement areas. Changes in the a/b ratio result in a change in the flow chamber's area and a reduction in the velocity from the elliptical gear to the flow meter body wall in this area. Based on these data, it was determined that elliptical gear design parameters lead to defects in CFD analysis flow rate calculations.

According to the results of the Taguchi L_9 analysis, the parameters a/b = 1.40, m = 2.50 mm, and z = 40 teeth, as well as a/b = 1.40, m = 2.50 mm, and z = 32 teeth are optimal for manufacturing flowmeters based on the signal-to-noise ratio obtained by taking the largest, best analysis into account.

Based on the analysis of the variance of the CFD models considering all variables during the flow meter experiments with a confidence level of 95 %, it was determined that the modulus value contributed the most with 65.25 %. In comparison, the a/b ratio contributed the least with 0.96 %. When the binary interactions of the flowmeter's parameters were considered, it was seen that the m*z variable had the greatest influence on the calculated flow rate at 17.28 %, while the a/b*pressure value had the least at 0.05 %. Based on the regression analysis results, it was established that the manufactured flowmeters had a reliability of R^2 = 99.00 %.

Under the percentage flow rate changes measured and assessed by CFD analysis, it was found that the largest percentage change occurred in the flow meter coded as Db-03 at 3.00 MPa pressure. In comparison, the slightest percentage change happened in the flow meter coded as Db-02 at 4.50 MPa pressure.

Funding

This study was supported by Gazi University Scientific Research Projects Coordination Unit (Project number: FDK - 2021–7425).

Author contributions

All authors contributed to the study's conception and design. Material preparation, data collection, and analysis were performed by İbrahim PAZARKAYA, Mehmet YAZAR, and Ahmet ÖZDEMİR. The first draft of the manuscript was written by İbrahim PAZARKAYA, and all authors commented on previous versions of the manuscript. All authors read and approved the final manuscript.

Declaration of competing interest

The authors declare that they have no known competing financial interests or personal relationships that could have appeared to influence the work reported in this paper.

Data availability

Data will be made available on request.

Acknowledgements

Authors thank The Scientific Research Projects Coordination Unit of Gazi University and The Academic Writing Application and Research Center of Gazi University.

The authors would like to thank Uyar Hidrolik San. Tic. Ltd. for assistance in the flow tests.

References

[1] A.M. Moinfar, G. Shahgholi, Y.A. Gilandeh, T.M. Gundoshmian, The effect of the tractor driving system on its performance and fuel consumption, Energy 202 (2020), 117803, https://doi.org/10.1016/j.energy.2020.117803.
[2] K. Rongping, Port Ship Energy Consumption Management Based on Beidou Satellite Communication[J], Jimei Univ., 2017.
[3] J. Yan, S. Li, R. Li, Numerical study on the auxiliary entrainment performance of an ejector with different area ratio, Appl. Therm. Eng. 185 (2021), 116369, https://doi.org/10.1016/j.applthermaleng.2020.116369.
[4] M. Meribout, A. Azzi, N. Ghendour, N. Kharoua, L. Khezzar, E. AlHosani, Multiphase flow meters targeting oil & gas industries, Meas. J. Int. Meas. Confed. 165 (2020), 108111, https://doi.org/10.1016/j.measurement.2020.108111.
[5] M. Addomine, G. Figliolini, E. Pennestrì, A landmark in the history of non-circular gears design: the mechanical masterpiece of Dondi's astrarium, Mech. Mach. Theor. 122 (2018) 219–232, https://doi.org/10.1016/j.mechmachtheory.2017.12.027.
[6] M.J. Lai, An Investigation of the Dynamic Behaviour of Systems with, Noncircular Gears, Cnkijournal, Beijing, 1996, pp. 377–388.
[7] Y.A. Yao, H.S. Yan, A new method for torque balancing of planar linkages using non-circular gears, Proc. Inst. Mech. Eng. Part C J. Mech. Eng. Sci. 217 (5) (2003) 495–503.
[8] D. Mundo, Geometric Design of Planetary Gear Train with Non-circular Gears, Mech. Mach. Theory Elsevier Ltd, 2006, pp. 456–472.
[9] S.L. Chang, C.B. Tsay, L.I. Wu, Mathematical model and undercutting analysis of elliptical gears generated by rack cutters, Mech. Mach. Theor. 31 (7) (1996) 879–890, https://doi.org/10.1016/0094-114X(95)00121-E.
[10] F.L. Litvin, A. Fuentes, Gear Geometry and Applied Theory, 2004.
[11] D.D. Chung, R. Wolfgramm, Maxillary arch perimeter prediction using Ramanujan's equation for the ellipse, Am. J. Orthod. Dentofacial Orthop. 147 (2) (2015) 235–241, https://doi.org/10.1016/j.ajodo.2014.10.022.
[12] İ. Pazarkaya, A. Özdemir, Eliptik dişli çarklarda bölüm elipsinin analitik olarak hesaplanması, in: Internatıonal Congress on Engıneerıng Scıences and Multıdıscıplınary Approaches, İstanbul, Turkey, 2021, pp. 490–498.
[13] M. Yazar, Ö. Ahmet, Computer-aıded desıgn, manufacture and experimental analysis of A paır of ellıptıcal spur gears, ANADOLU Univ. J. Sci. Technol. A - Appl. Sci. Eng. 17 (5) (2016) 869, https://doi.org/10.18038/aubtda.279855.
[14] İ. Pazarkaya, M. Yazar, A. Özdemir, Elliptical gear design, manufacturing, analysis, and their industrial practises, Gazi Üniversitesi Fen Bilim. Derg. Part C Tasarım ve Teknol. 10 (3) (2022) 558–576, https://doi.org/10.29109/gujsc.1103492.
[15] B.W. Bair, Computer aided design of elliptical gears with circular-arc teeth, Mech. Mach. Theor. 39 (2) (Feb. 2004) 153–168, https://doi.org/10.1016/S0094-114X(03)00111-3.
[16] H. Jiang, D.Z. Li, X. Lian, B.C. Jiang, CADDM Research on Design Method of Non-circular Gear Pair with Double Generating Angles, 2015.
[17] N. Ertürk, A. Vernet, J. Pallares, R. Castilla, G. Raush, Small-scale characteristics and turbulent statistics of the flow in an external gear pump by time-resolved PIV, Flow Meas. Instrum. 29 (2013) 52–60, https://doi.org/10.1016/j.flowmeasinst.2012.09.004.
[18] G.S. Lee, M.Y. Park, Flow field characterıstıcs in the housıng of noncırcular gear flowmeter, in: 6th International Conference on Heat Transfer, Fluid Mechanics and Thermodynamics, 2008, p. LG1.

[19] K. Zhou, D. She, X. Li, Analysis of high-order elliptic gear transmission and its application in flowmeter, in: ACM International Conference Proceeding Series, 2021, pp. 260–266, https://doi.org/10.1145/3480571.3480618.
[20] Q. Zeng, J. Sun, Analysis of Flow of Outer Meshing Elliptic Gear Pump Based on Fluent, Aest, 2016, pp. 374–379, https://doi.org/10.2991/aest-16.2016.49.
[21] A.N.S.Y.S. Fluent, ANSYS Fluent 12.0 Theory Guide, ANSYS Inc., Canonsburg, PA., 2009.
[22] F. Litvin, A. Fuentes-Aznar, Noncircular Gears: Design and Generation, Cambridge Univ. Press, New York, 2009.
[23] R. Cebeci, St-37 Ve St- 52 Sac Malzemelerin Lazerle Kesilmesinde İşleme Parametrelerinin Kesim Kalitesine Etkisinin İncelenmesi, Karabük Üniversitesi, 2021.
[24] M. Pul, Comparison of Surface Roughness and Tool Wear in Turning of 7075, 6061 and 2024 Aluminum Alloys, *Int. J. Eng. Res. Dev.* 9 (2) (2017) 65–75, https://doi.org/10.29137/umagd.351746.
[25] L.V. Vanegas-Useche, M.M. Abdel-Wahab, G.A. Parker, Nuevo par de engranajes no circulares para reducir las aceleraciones del eje: comparación con engranajes sinusoidales y elípticos, Dyna 83 (Sep. 2016) 220–228, https://doi.org/10.15446/dyna.v83n198.49170, 198.